Characterization and Manipulation of Intervalley Scattering Induced by an Individual Monovacancy in Graphene

Yu Zhang,[1,2,3,*,†] Fei Gao,[4,*] Shiwu Gao,[5] Mads Brandbyge,[4] and Lin He[3,‡]

[1]School of Integrated Circuits and Electronics, MIIT Key Laboratory for Low-Dimensional Quantum Structure and Devices, Beijing Institute of Technology, Beijing 100081, China

[2]Advanced Research Institute of Multidisciplinary Sciences, Beijing Institute of Technology, Beijing 100081, China

[3]Center for Advanced Quantum Studies, Department of Physics, Beijing Normal University, 100875 Beijing, China

[4]Center for Nanostructured Graphene, Department of Physics, Technical University of Denmark, DK-2800 Kongens Lyngby, Denmark

[5]Beijing Computational Science Research Center, 100193 Beijing, China

(Received 11 April 2022; accepted 29 July 2022; published 23 August 2022)

Intervalley scattering involves microscopic processes that electrons are scattered by atomic-scale defects on the nanoscale. Although central to our understanding of electronic properties of materials, direct characterization and manipulation of range and strength of the intervalley scattering induced by an individual atomic defect have so far been elusive. Using scanning tunneling microscope, we visualize and control intervalley scattering from an individual monovacancy in graphene. By directly imaging the affected range of monovacancy-induced intervalley scattering, we demonstrate that it is inversely proportional to the energy; i.e., it is proportional to the wavelength of massless Dirac fermions. A giant electron-hole asymmetry of the intervalley scattering is observed because the monovacancy is charged. By further charging the monovacancy, the bended electronic potential around the monovacancy softens the scattering potential, which, consequently, suppresses the intervalley scattering of the monovacancy.

DOI: 10.1103/PhysRevLett.129.096402

Exploring the nature of emergent physical phenomena induced by atomic defects requires nanoscale measurements. One representative example is the monovacancy-induced local magnetism in graphene. Early transport and magnetic measurements of mesoscopic graphene samples with amount of vacancies reported either Kondo effect or spin-half paramagnetism, confirming the existence of local magnetism in these systems [1,2]. However, the measured magnetic moment per monovacancy was only $\sim 0.1\mu_B$, much smaller than $\sim 1.5\mu_B$ predicted in theory [3]. Later, nanoscale spectroscopy studies on an individual monovacancy revealed different magnetic states [4–6], helping us to understand the much smaller magnetic moment in mesoscopic measurements. Moreover, nanoscale measurements on atomic defect may reveal results beyond that in mesoscopic measurements. Recent experiments demonstrate that the local wave front dislocations induced by an individual atomic impurity reveal Berry phase signatures of the system [7–9].

Besides the local magnetism, the most relevant electronic property induced by monovacancy in graphene is the intervalley scattering. In pristine graphene, electrons have valley degree of freedom, providing the opportunity of information coding and processing [10–14]. However, atomic defects can generate intervalley scattering [15–32], which greatly limits the ability to manipulate the valley. Previous studies on defect-induced intervalley scattering mainly relied on mesoscopic transport measurements [25–36]. However, the scattering centers in transport measurements are always random and disordered, and their types and charge states are indistinguishable, owing to the lack of spatial resolution. In such a case, many seemingly contradictory phenomena were observed in transport measurements, including weak localization and weak antilocalization [25,26], as well as electron-hole symmetry and asymmetry effects [32,35,36], which need further exploration. In this Letter, we report nanoscale probing of intervalley scattering induced by an individual monovacancy in graphene via scanning tunneling microscopy (STM) and scanning tunneling spectroscopy (STS). Our experiment indicates that the affected range of monovacancy-induced intervalley scattering is proportional to the wavelength of massless Dirac fermions in graphene. A giant electron-hole asymmetry of intervalley scattering is observed because the monovacancy is charged. By further charging the monovacancy, the scattering potential around the monovacancy is softened and, consequently, suppresses the intervalley scattering. Our results provide an in-depth understanding of rich transport phenomena from a microscopic point of view.

In our experiments, multilayer graphene with monovacancies is directly synthesized on Ni foils via chemical vapor deposition, and then it is transferred onto a SiO_2/Si wafer (see Methods and Fig. S1 in Supplemental Material [37]). There is usually a rotational misalignment between the graphene layers, resulting in moiré patterns in STM

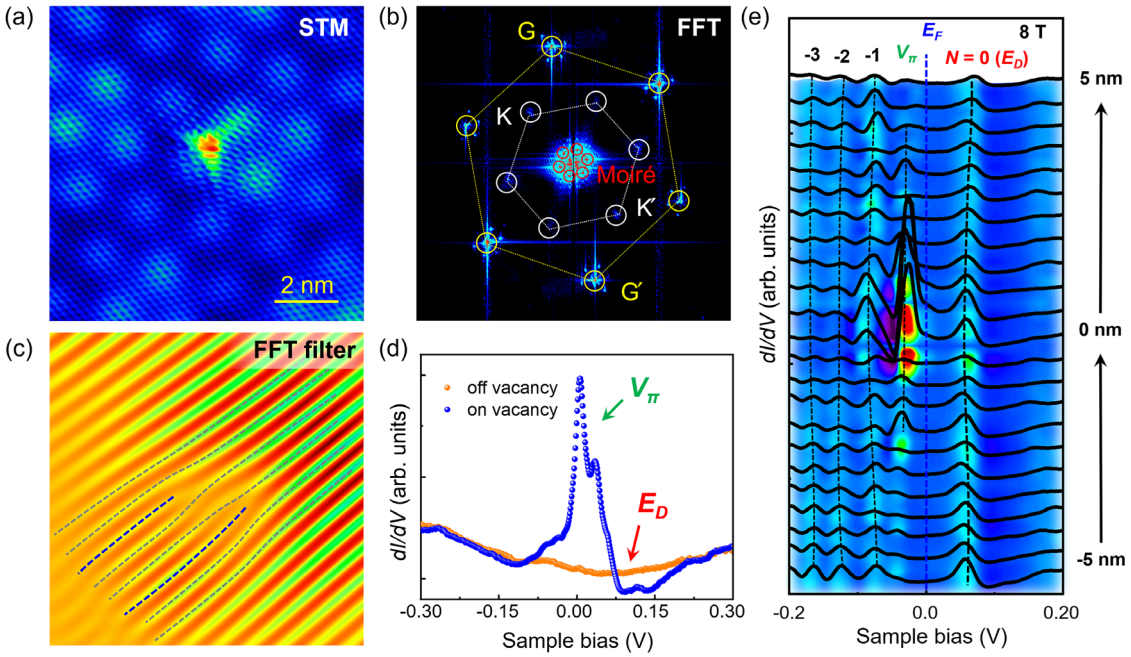

FIG. 1. (a), (b) Atomic resolution STM image and corresponding FFT image of a monovacancy in TBG. (c) FFT-filtered STM image along a specific direction of the intervalley scattering. (d) Typical STS spectra recorded on and off the monovacancy under 0 T. The V_π state and E_D are marked. (e) The evolution of STS spectra recorded across the monovacancy under 8 T. The monovacancy locates at 0 nm. The Landau level indices are marked.

images. Figure 1(a) shows a representative STM image of a monovacancy in the topmost graphene layer of twisted bilayer graphene (TBG) with the twist angle $\theta \approx 6°$. The two graphene layers are electronically decoupled [45–51], which can be experimentally verified by the π Berry phase signature and Landau level spectroscopy, as illustrated subsequently.

The atomic-resolution STM image of a monovacancy in the AB-stacked region of TBG exhibits a distinctive triangular $\sqrt{3} \times \sqrt{3}R30°$ interference pattern [Fig. 1(a)], which is similar to that in single-layer graphene (SLG) [4–6,52,53]. The location of the monovacancy has almost no influence on the studied phenomena in our current work, owing to the electronic decoupling of the topmost graphene sheet [45–51]. Figure 1(b) shows the fast Fourier transform (FFT) image of Fig. 1(a). The outer (inner) six bright spots are the reciprocal lattice of the topmost SLG (TBG), and the middle six bright spots located at K and K' valleys arise from the monovacancy-induced intervalley scattering. From the inverse FFT by filtering a pair of K and K' valleys, we find the number of additional wave fronts N is always 2 around the monovacancy, as highlighted by blue dashed lines in Fig. 1(c), which is attributed to the rotation of sublattice pseudospin during the intervalley scattering process and is a signature of π Berry phase [7–9]. Therefore, our experiments demonstrate that the topmost graphene layer behaves as a SLG.

Now we explore the electronic properties around an individual monovacancy in graphene under perpendicular magnetic fields B. Figures 1(d) and 1(e) show spatially resolved STS spectra recorded across the monovacancy under $B = 0$ and 8 T, respectively (see Fig. S2 for more data [37]). Away from the monovacancy, the STS spectra

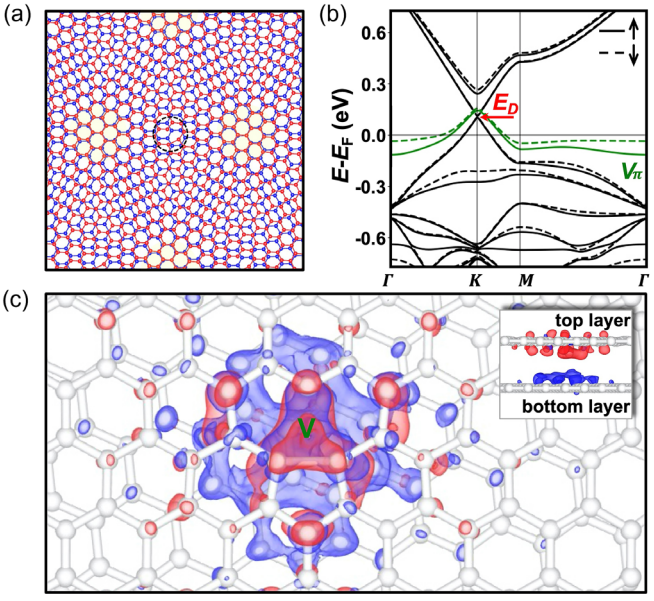

FIG. 2. (a) Atomic structure of TBG with $\theta \approx 6°$. A monovacancy is located at the AB-stacked region of TBG, as marked by the black circle. The red and blue spheres indicate C atoms of the topmost and underlying graphene layers, respectively. (b) Band structure of a monovacancy in TBG. (c) Δ_ρ around the monovacancy with the isosurface value of 0.0015 $e/\text{Å}^3$. Red and blue clouds indicate the electron accumulation and depletion, respectively.

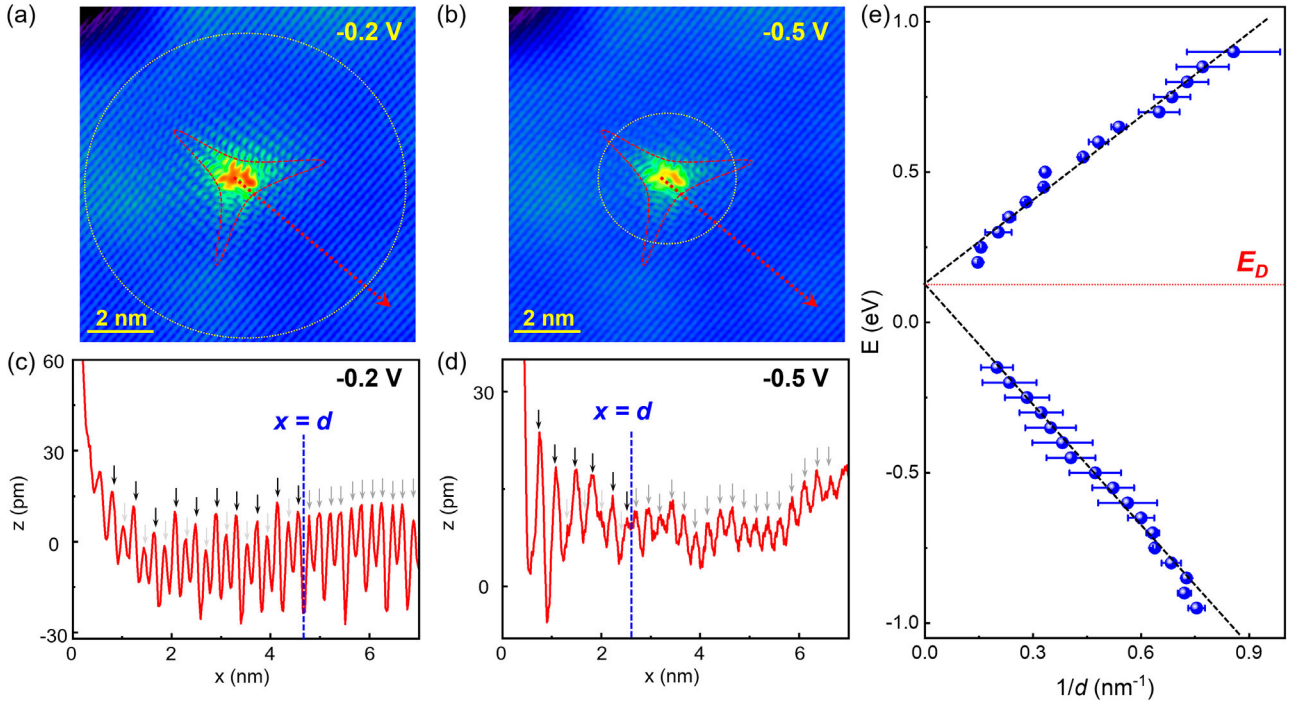

FIG. 3. (a), (b) STM images of a monovacancy in TBG acquired at −0.2 and −0.5 V with 512 × 512 pixels, respectively. The yellow dashed circles indicate the ranges of monovacancy-induced intervalley scattering. (c), (d) Line profiles of the red arrows in (a) and (b). The arrows indicate the locations of the carbon atoms in the topmost graphene layer. The alternate heights marked by black and light gray arrows for $x < d$ imply the existence of signal from the intervalley scattering, while the homogeneous heights marked by dark gray arrows for $x > d$ imply the negligible signal from the intervalley scattering. The $x = d$ is the length of the intervalley scattering, determined as the position when the difference of the apparent heights between two adjacent carbon atoms is less than 1 pm or the apparent heights no longer follow the rule of alternation. (e) A linear relation between $(E - E_D)$ and $1/d$.

exhibit a typical V shape under 0 T, together with the Landau quantization of massless Dirac fermions under 8 T, implying the two graphene layers are decoupled [46–51]. As approaching to the monovacancy, the monovacancy-induced V_π state gradually appears and splits into two spin-polarized states [3,5]. In the following, we mainly focus on the energy of the V_π state. We find the V_π state in TBG usually lies at several tens of meV below the Dirac point E_D, which is quite different from that in the SLG where the V_π state is just at E_D [3].

To understand such a phenomenon, we carry out density functional theory (DFT) calculations of a monovacancy in the AB-stacked region of TBG with $\theta \approx 6°$. As shown in Fig. 2, the monovacancy-induced V_π state in TBG always lies below E_D and exhibits site-independent features, which are consistent with our experiments. To gain further insight, we calculate the spatially resolved charge density difference Δ_ρ around the monovacancy, which can intuitively reflect the monovacancy-induced interlayer charge transfer in TBG (see Supplemental Material [37]). From Fig. 2(c), we can observe an obvious electron transfer from the underlying to the topmost layer of TBG around the monovacancy, which is the root cause of the energy-separated V_π state and E_D.

Now we concentrate on the spatial distribution of monovacancy-induced intervalley scattering in TBG. Figures 3(a) and 3(b) show STM images recorded under 0 T at the sample bias of −0.2 and −0.5 V, respectively. The range of the monovacancy-induced intervalley scattering d can be defined from the real-space STM images as the distance from the monovacancy to the scattering termination point where the $\sqrt{3} \times \sqrt{3}$ interference patterns are absent, as marked in Figs. 3(c) and 3(d), respectively (the values d acquired in STM images and STS mappings are almost the same; more details are given in Figs. S3–S5 [37]). When approaching the vacancy E_D, the range of monovacancy-induced intervalley scattering significantly increases and extends to the whole 15×15 nm^2 STM images when reaching E_D (Fig. S6 [37]). The measured electron energy E versus $1/d$ is summarized in Fig. 3(e), which exhibits a linear relationship. Taking into account the linear dispersion of the charge carriers in graphene, our result indicates that the affected range of intervalley scattering by an individual monovacancy is proportional to the wavelength of massless Dirac fermions. Therefore, the intervalley scattering of mesoscopic graphene samples with a certain density of monovacancies can be much enhanced when the Fermi energy E_F is near E_D. This result explains the origin of the transition from weak localization to weak antilocalization in graphene when the energy of carriers is tuned away from E_D in previous transport

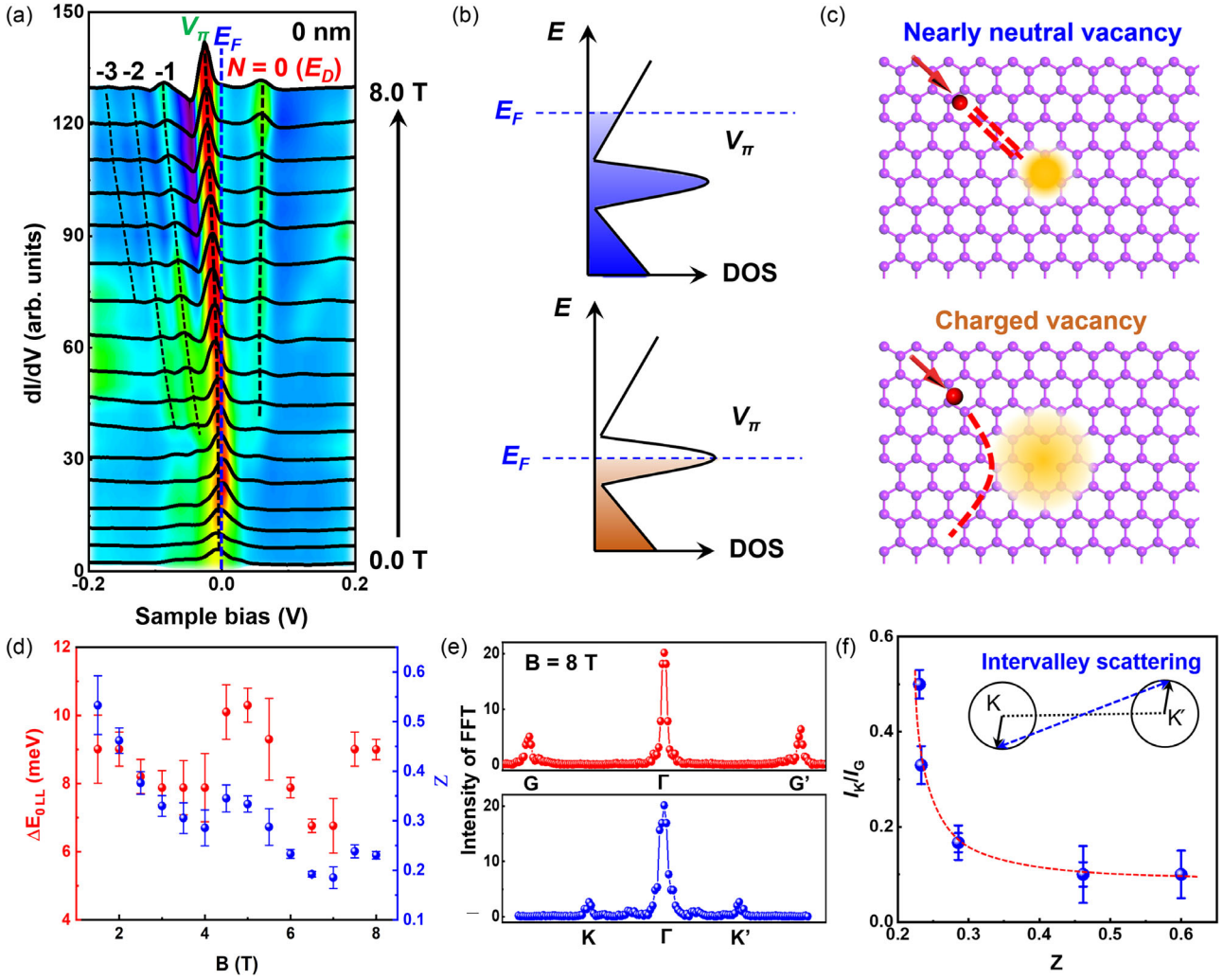

FIG. 4. (a) The evolution of STS spectra recorded at the monovacancy as a function of B. The V_π states, E_D, E_F, and the Landau level indices are labeled. (b) Schematic DOS at the monovacancy in TBG. The V_π state is partially filled under 0 T, implying the monovacancy is charged. As increasing B, the V_π state is gradually filled and finally fully filled under 8 T, implying the monovacancy is nearly neutral. (c) Schematic scattering of carriers induced by neutral and charged monovacancy. (d) $\Delta E_{0\,\mathrm{LL}}$ and Z as a function of B. (e) Line profiles along the directions of G-Γ-G' and K-Γ-K' in the FFT images at 0.5 V under 8 T. (f) I_K/I_G versus Z. Inset: Schematic of intervalley scattering.

measurements [54]. Moreover, the absolute values of slopes for E versus $1/d$ are 0.90 and 1.32 for electrons and holes, respectively. Such a giant electron-hole asymmetry of the intervalley scattering is attributed to the fact that the monovacancy is charged, thus resulting in the charge carriers being scattered more strongly when they are attracted to the charged defect than when they are repelled from it.

Theoretically, the charge state of the monovacancy in graphene can be tuned by doping the V_π state. In our experiments, the charge state of monovacancy can be reversibly tuned by perpendicular magnetic fields. Figure 4(a) shows representative STS spectra acquired at the monovacancy as a function of B from 0 to 8 T. Apart from the evolution of the Landau levels, the V_π state becomes more localized as increasing B. Moreover, the V_π state trends to monotonously shift from −7 meV under $B = 0$ T toward a lower energy, and reaches the minimum of −26 meV under $B = 8$ T, as shown in Fig. 4(a). Such a phenomenon, on the one hand, is attributed to the redistribution of electronic states of graphene beneath the STM tip that are generated by the confinements of tip-induced electronic potentials and external magnetic fields (Fig. S7 [37]), as demonstrated recently [55–64]. On the other hand, is attributed to the existence of electron transfers between the adjacent two graphene sheets around the defect, based on our STS measurements (Fig. 1) and DFT calculations (Fig. 2).

Theoretically, a monovacancy in graphene can host a local positive charge [48,65,66]. As shown in Figs. 4(b) and 4(c), the monovacancy is expected to be neutral when the V_π state is fully filled, and is gradually charged with the V_π state shifting across E_F [34]. In our experiments, the charge states of a monovacancy under B can be

precisely monitored by the spatial-resolved Landau level spectroscopy. As shown in Fig. 1(e), we can observe an energy down-shift of $N = 0$ LL, $\Delta E_{0\,\mathrm{LL}}$, near the monovacancy relative to its value far away. $\Delta E_{0\,\mathrm{LL}}$ can be derived from the screening of a charged monovacancy as $\Delta E_{0\,\mathrm{LL}} \approx -(Z/\kappa)[e^2/(4\sqrt{2\pi}\varepsilon_0 l_B)]$. Here ε_0 is the permittivity of free space, e is the electron charge, $l_B = \sqrt{\hbar/(eB)}$ is the magnetic length, $\hbar$ is the reduced Planck constant, and κ is the effective dielectric constant [48,66,67]. Therefore, the charge state Z of the monovacancy in graphene under various B can be precisely extracted, as summarized in Fig. 4(d). Obviously, the Z shows an approximately monotonous decreasing from 0.5 to 0.2 as B increases from 1.5 to 8.0 T, and can be extrapolated to $Z \approx 0.6$ when $B = 0$ T.

The intensity of monovacancy-induced intervalley scattering in graphene can be strongly influenced by the charge states. By charging the monovacancy, the monovacancy-induced scattering potential is softened from atomically sharp to long-range, which efficiently suppresses the intervalley scattering [Fig. 4(c)]. Figure 4(e) shows line profiles along the directions of G-Γ-G' and K-Γ-K' in FFT images acquired from STS maps under $B = 8$ T at 0.5 V (Fig. S8 [37]). The intensity ratio of intervalley scattering I_K and reciprocal lattice I_G, I_K/I_G, as a function of Z is summarized in Fig. 4(f). As Z decreases, I_K/I_G gradually enhances, together with the increasing range of $\sqrt{3} \times \sqrt{3}$ interference patterns in real space. Our results explicitly verify that the intensity of monovacancy-induced intervalley scattering is strongly suppressed when the monovacancy is charged, as schematically shown in Fig. 4(c).

In summary, we directly image the intervalley scattering induced by an individual monovacancy in graphene. The affected range of monovacancy-induced intervalley scattering is proportional to the wavelength of massless Dirac fermions in graphene, accompanied by a giant electron-hole asymmetry. By further charging the monovacancy, the scattering potential around the monovacancy is softened and, consequently, suppresses the intervalley scattering. Our results pave the way to control the intervalley scattering in multivalley systems, promoting the development of valleytronics.

This work was supported by the National Key R and D Program of China (No. 2021YFA1401900 and No. 2021YFA1400100), National Natural Science Foundation of China (No. 12141401 and No. 11974050), and the China Postdoctoral Science Foundation (No. 2021M700407).

*Y. Z and F. G. contributed equally to this work.
†Corresponding author.
yzhang@bit.edu.cn
‡Corresponding author.
helin@bnu.edu.cn

[1] J. Chen, L. Li, W. G. Cullen, E. D. Williams, and M. S. Fuhrer, Tunable Kondo effect in graphene with defects, Nat. Phys. **7**, 535 (2011).
[2] R. R. Nair, M. Sepioni, I. Tsai, O. Lehtinen, J. Keinonen, A. V. Krasheninnikov, T. Thomson, A. K. Geim, and I. V. Grigorieva, Spin-half paramagnetism in graphene induced by point defects, Nat. Phys. **8**, 199 (2012).
[3] O. V. Yazyev and L. Helm, Defect-induced magnetism in graphene, Phys. Rev. B **75**, 125408 (2007).
[4] Y. Jiang, P. Lo, D. May, G. Li, G. Guo, F. B. Anders, T. Taniguchi, K. Watanabe, J. Mao, and E. Y. Andrei, Inducing Kondo screening of vacancy magnetic moments in graphene with gating and local curvature, Nat. Commun. **9**, 2349 (2018).
[5] Y. Zhang, S. Li, H. Huang, W. Li, J. Qiao, W. Wang, L. Yin, K. Bai, W. Duan, and L. He, Scanning Tunneling Microscopy of the π Magnetism of a Single Carbon Vacancy in Graphene, Phys. Rev. Lett. **117**, 166801 (2016).
[6] Y. Zhang, F. Gao, S. Gao, and L. He, Tunable magnetism of a single-carbon vacancy in graphene, Sci. Bull. **65**, 194 (2020).
[7] C. Dutreix, H. González-Herrero, I. Brihuega, M. I. Katsnelson, C. Chapelier, and V. T. Renard, Measuring the Berry phase of graphene from wavefront dislocations in Friedel oscillations, Nature (London) **574**, 219 (2019).
[8] Y. Zhang, Y. Su, and L. He, Intervalley Quantum Interference and Measurement of Berry Phase in Bilayer Graphene, Phys. Rev. Lett. **125**, 116804 (2020).
[9] Y. Zhang, Y. Su, and L. He, Quantum interferences of pseudospin-mediated atomic-scale vortices in monolayer graphene, Nano Lett. **21**, 2526 (2021).
[10] A. Rycerz, J. Tworzydlo, and C. W. J. Beenakker, Valley filter and valley valve in graphene, Nat. Phys. **3**, 172 (2007).
[11] D. Xiao, W. Yao, and Q. Niu, Valley-Contrasting Physics in Graphene: Magnetic Moment and Topological Transport, Phys. Rev. Lett. **99**, 236809 (2007).
[12] D. Pesin and A. H. MacDonald, Spintronics and pseudospintronics in graphene and topological insulators, Nat. Mater. **11**, 409 (2012).
[13] X. Xu, W. Yao, D. Xiao, and T. F. Heinz, Spin and pseudospins in layered transition metal dichalcogenides, Nat. Phys. **10**, 343 (2014).
[14] J. R. Schaibley, H. Yu, G. Clark, P. Rivera, J. S. Ross, K. L. Seyler, W. Yao, and X. Xu, Valleytronics in 2D materials, Nat. Rev. Mater. **1**, 16055 (2016).
[15] J. H. Chen, W. G. Cullen, C. Jang, M. S. Fuhrer, and E. D. Williams, Defect Scattering in Graphene, Phys. Rev. Lett. **102**, 236805 (2009).
[16] T. O. Wehling, S. Yuan, A. I. Lichtenstein, A. K. Geim, and M. I. Katsnelson, Resonant Scattering by Realistic Impurities in Graphene, Phys. Rev. Lett. **105**, 056802 (2010).
[17] N. M. R. Peres, Colloquium: The transport properties of graphene: An introduction, Rev. Mod. Phys. **82**, 2673 (2010).
[18] C. Bena, Effect of a Single Localized Impurity on the Local Density of States in Monolayer and Bilayer Graphene, Phys. Rev. Lett. **100**, 076601 (2008).
[19] P. Mallet, I. Brihuega, S. Bose, M. M. Ugeda, J. M. Gomez-Rodrıguez, K. Kern, and J. Y. Veuillen, Role of pseudospin in quasiparticle interferences in epitaxial graphene probed

by high-resolution scanning tunneling microscopy, Phys. Rev. B **86**, 045444 (2012).
[20] C. Dutreix and M. I. Katsnelson, Friedel oscillations at the surfaces of rhombohedral N-layer graphene, Phys. Rev. B **93**, 035413 (2016).
[21] F. Joucken, C. Bena, Z. Ge, E. Quezada-Lopez, S. Pinon, V. Kaladzhyan, T. Taniguchi, K. Watanabe, A. Ferreira, and J. Velasco Jr, Direct visualization of native defects in graphite and their effect on the electronic properties of Bernal-stacked bilayer graphene, Nano Lett. **21**, 7100 (2021).
[22] G. M. Rutter, J. N. Crain, N. P. Guisinger, T. Li, P. N. First, and J. A. Stroscio, Scattering and interference in epitaxial graphene, Science **317**, 219 (2007).
[23] I. Brihuega, P. Mallet, C. Bena, S. Bose, C. Michaelis, L. Vitali, F. Varchon, L. Magaud, K. Kern, and J. Y. Veuillen, Quasiparticle Chirality in Epitaxial Graphene Probed at the Nanometer Scale, Phys. Rev. Lett. **101**, 206802 (2008).
[24] H. Yan, C. Liu, K. Bai, X. Wang, M. Liu, W. Yan, L. Meng, Y. Zhang, Z. Liu, R. Dou, J. Nie, Y. Yao, and L. He, Electronic structures of graphene layers on a metal foil: The effect of atomic-scale defects, Appl. Phys. Lett. **103**, 143120 (2013).
[25] S. V. Morozov, K. S. Novoselov, M. I. Katsnelson, F. Schedin, L. A. Ponomarenko, D. Jiang, and A. K. Geim, Strong Suppression of Weak Localization in Graphene, Phys. Rev. Lett. **97**, 016801 (2006).
[26] X. Wu, X. Li, Z. Song, C. Berger, and W. A. de Heer, Weak Antilocalization in Epitaxial Graphene: Evidence for Chiral Electrons, Phys. Rev. Lett. **98**, 136801 (2007).
[27] D. W. Horsell, F. V. Tikhonenko, R. V. Gorbachev, and A. K. Savchenko, Weak localization in monolayer and bilayer graphene, Phil. Trans. R. Soc. A **366**, 245 (2008).
[28] A. Khademi, K. Kaasbjerg, P. Dosanjh, A. Stöhr, S. Forti, U. Starke, and J. A. Folk, Weak localization measurements of electronic scattering rates in Li-doped epitaxial graphene, Phys. Rev. B **100**, 161405(R) (2019).
[29] E. McCann, K. Kechedzhi, V. I. Falko, H. Suzuura, T. Ando, and B. L. Altshuler, Weak-Localization Magnetoresistance and Valley Symmetry in Graphene, Phys. Rev. Lett. **97**, 146805 (2006).
[30] A. F. Morpurgo and F. Guinea, Intervalley Scattering, Long-Range Disorder, and Effective Time-Reversal Symmetry Breaking in Graphene, Phys. Rev. Lett. **97**, 196804 (2006).
[31] V. I. Falko, K. Kechedzhi, E. McCann, B. L. Altshuler, H. Suzuura, and T. Ando, Weak localization in graphene, Solid State Commun. **143**, 33 (2007).
[32] J. H. Chen, C. Jang, S. Adam, M. S. Fuhrer, E. D. Williams, and M. Ishigami, Charged-impurity scattering in graphene, Nat. Phys. **4**, 377 (2008).
[33] M. Li, C. Tang, D. C. Ling, L. J. Li, C. C. Chi, and J. Chen, Charged impurity-induced scatterings in chemical vapor deposited graphene, J. Appl. Phys. **114**, 233703 (2013).
[34] B. Yan, Q. Han, Z. Jia, J. Niu, T. Cai, D. Yu, and X. Wu, Electrical control of intervalley scattering in graphene via the charge state of defects, Phys. Rev. B **93**, 041407(R) (2016).
[35] M. Monteverde, C. Ojeda-Aristizabal, R. Weil, K. Bennaceur, M. Ferrier, S. Gueron, C. Glattli, H. Bouchiat, J. N. Fuchs, and D. L. Maslov, Transport and Elastic Scattering Times as Probes of the Nature of Impurity Scattering in Single-Layer and Bilayer Graphene, Phys. Rev. Lett. **104**, 126801 (2010).
[36] J. Li, L. Lin, D. Rui, Q. Li, J. Zhang, N. Kang, Y. Zhang, H. Peng, Z. Liu, and H. Q. Xu, Electron-hole symmetry breaking in charge transport in nitrogen-doped graphene, ACS Nano **11**, 4641 (2017).
[37] See Supplemental Material at http://link.aps.org/supplemental/10.1103/PhysRevLett.129.096402 for methods, more STM images, STS spectra, and details of the analysis, which includes Refs. [38–44].
[38] J. P. Perdew, K. Burke, and M. Ernzerhof, Generalized Gradient Approximation Made Simple, Phys. Rev. Lett. **77**, 3865 (1996).
[39] J. Klimeš, D. R. Bowler, and A. Michaelides, Chemical accuracy for the van der Waals density functional, J. Phys. Condens. Matter **22**, 022201 (2009).
[40] M. Brandbyge, J. Mozos, P. Ordejón, J. Taylor, and K. Stokbro, Density-functional method for nonequilibrium electron transport, Phys. Rev. B **65**, 165401 (2002).
[41] J. M. Soler, E. Artacho, J. D. Gale, A. García, J. Junquera, P. Ordejón, and D. Sánchez-Portal, The SIESTA method for *ab initio* order-N materials simulation, J. Phys. Condens. Matter **14**, 2745 (2002).
[42] N. Papior, N. Lorente, T. Frederiksen, A. García, and M. Brandbyge, Improvements on non-equilibrium and transport Green function techniques: The next-generation transiesta, Comput. Phys. Commun. **212**, 8 (2017).
[43] L. Bengtsson, Dipole correction for surface supercell calculations, Phys. Rev. B **59**, 12301 (1999).
[44] N. Papior, sisl: v0.9.4, 2018, 10.5281/zenodo.597181.
[45] W. Yan, L. Meng, M. Liu, J. Qiao, Z. Chu, R. Dou, Z. Liu, J. Nie, D. G. Naugle, and L. He, Angle-dependent van Hove singularities and their breakdown in twisted graphene bilayers, Phys. Rev. B **90**, 11540 (2014).
[46] D. L. Miller, K. D. Kubista, G. M. Rutter, M. Ruan, W. A. de Heer, P. N. First, and J. A. Stroscio, Observing the quantization of zero mass carriers in graphene, Science **324**, 924 (2009).
[47] Y. J. Song, A. F. Otte, Y. Kuk, Y. Hu, D. B. Torrance, P. N. First, W. A. de Heer, H. Min, S. Adam, M. D. Stiles, A. H. MacDonald, and J. A. Stroscio, High-resolution tunnelling spectroscopy of a graphene quartet, Nature (London) **467**, 185 (2010).
[48] M. O. Goerbig, Electronic properties of graphene in a strong magnetic field, Rev. Mod. Phys. **83**, 1193 (2011).
[49] A. Luican, G. Li, A. Reina, J. Kong, R. R. Nair, K. S. Novoselov, A. K. Geim, and E. Y. Andrei, Single-Layer Behavior and Its Breakdown in Twisted Graphene Layers, Phys. Rev. Lett. **106**, 126802 (2011).
[50] L. Yin, S. Li, J. Qiao, J. Nie, and L. He, Landau quantization in graphene monolayer, Bernal bilayer, and Bernal trilayer on graphite surface, Phys. Rev. B **91**, 115405 (2015).
[51] S. Li, Y. Zhang, L. Yin, and L. He, Scanning tunneling microscope study of quantum Hall isospin ferromagnetic states in the zero Landau level in a graphene monolayer, Phys. Rev. B **100**, 085437 (2019).
[52] M. M. Ugeda, I. Brihuega, F. Guinea, and J. M. Gomez-Rodrıguez, Missing Atom as a Source of Carbon Magnetism, Phys. Rev. Lett. **104**, 096804 (2010).

[53] J. Mao, Y. Jiang, D. Moldovan, G. Li, K. Watanabe, T. Taniguchi, M. R. Masir, F. M. Peeters, and E. Y. Andrei, Realization of a tunable artificial atom at a supercritically charged vacancy in graphene, Nat. Phys. **12**, 545 (2016).
[54] Z. Liao, B. Han, H. Wu, and D. Yu, Gate voltage dependence of weak localization in bilayer graphene, Appl. Phys. Lett. **97**, 163110 (2010).
[55] Y. Ren, Q. Cheng, S. Li, C. Yan, Y. Liu, K. Lv, M. Zhang, Q. Sun, and L. He, Spatial and magnetic confinement of massless Dirac fermions, Phys. Rev. B **104**, L161408 (2021).
[56] Y. Zhao, J. Wyrick, F. D. Natterer, J. F. Rodriguez-Nieva, C. Lewandowski, K. Watanabe, T. Taniguchi, L. S. Levitov, N. B. Zhitenev, and J. A. Stroscio, Creating and probing electron whispering-gallery modes in graphene, Science **348**, 672 (2015).
[57] F. Ghahari, D. Walkup, C. Gutiérrez, J. F. Rodriguez-Nieva, Y. Zhao, J. Wyrick, F. D. Natterer, W. G. Cullen, K. Watanabe, T. Taniguchi, L. S. Levitov, N. B. Zhitenev, and J. A. Stroscio, An on/off Berry phase switch in circular graphene resonators, Science **356**, 845 (2017).
[58] C. Gutiérrez, D. Walkup, F. Ghahari, C. Lewandowski, J. F. Rodriguez-Nieva, K. Watanabe, T. Taniguchi, L. S. Levitov, N. B. Zhitenev, and J. A. Stroscio, Interaction-driven quantum Hall wedding cake-like structures in graphene quantum dots, Science **361**, 789 (2018).
[59] N. M. Freitag, T. Reisch, L. A. Chizhova, P. Nemes-Incze, C. Holl, C. R. Woods, R. V. Gorbachev, Y. Cao, A. K. Geim, K. S. Novoselov, J. Burgdörfer, F. Libisch, and M. Morgenstern, Large tunable valley splitting in edge-free graphene quantum dots on boron nitride, Nat. Nanotechnol. **13**, 392 (2018).
[60] G. V. Nazin, X. H. Qiu, and W. Ho, Charging and Interaction of Individual Impurities in a Monolayer Organic Crystal, Phys. Rev. Lett. **95**, 166103 (2005).
[61] F. Marczinowski, J. Wiebe, F. Meier, K. Hashimoto, and R. Wiesendange, Effect of charge manipulation on scanning tunneling spectra of single Mn acceptors in InAs, Phys. Rev. B **77**, 115318 (2008).
[62] V. W. Brar, R. Decker, H. Solowan, Y. Wang, L. Maserati, K. T. Chan, H. Lee, C. O. Girit, A. Zettl, S. G. Louie, M. L. Cohen, and M. F. Crommie, Gate-controlled ionization and screening of cobalt adatoms on a graphene surface, Nat. Phys. **7**, 43 (2011).
[63] Y. Wang, V. W. Brar, A. V. Shytov, Q. Wu, W. Regan, H. Tsai, A. Zettl, L. S. Levitov, and M. F. Crommie, Mapping Dirac quasiparticles near a single Coulomb impurity on graphene, Nat. Phys. **8**, 653 (2012).
[64] I. Fernandez-Torrente, D. Kreikemeyer-Lorenzo, A. Strozecka, K. J. Franke, and J. I. Pascual, Gating the Charge State of Single Molecules by Local Electric Fields, Phys. Rev. Lett. **108**, 036801 (2012).
[65] Y. Liu, M. Weinert, and L. Li, Determining charge state of graphene vacancy by noncontact atomic force microscopy and first-principles calculations, Nanotechnology **26**, 035702 (2015).
[66] A. Luican-Mayer, M. Kharitonov, G. Li, C. Lu, I. Skachko, A. B. Gonçalves, K. Watanabe, T. Taniguchi, and Eva Y. Andrei, Screening Charged Impurities and Lifting the Orbital Degeneracy in Graphene by Populating Landau Levels, Phys. Rev. Lett. **112**, 036804 (2014).
[67] O. O. Sobol, P. K. Pyatkovskiy, E. V. Gorbar, and V. P. Gusynin, Screening of a charged impurity in graphene in a magnetic field, Phys. Rev. B **94**, 115409 (2016).